Wavefront control simulations for the Giant Magellan Telescope: Field-dependent segment piston control

Fernando Quirós-Pacheco[a], Rodolphe Conan[a], Brian McLeod[b], Benjamin Irarrazaval[a], and Antonin Bouchez[a]

[a]GMTO Organization, 465 North Halstead St, Suite 250, Pasadena, CA 91107, USA
[b]Smithsonian Astrophysical Observatory, 60 Garden St, MS 20, Cambridge, MA 02138, USA

ABSTRACT

We present in this paper preliminary simulation results aimed at validating the GMT piston control strategy. We will in particular consider an observing mode in which an Adaptive Optics (AO) system is providing fast on-axis WF correction with the Adaptive Secondary Mirror (ASM), while the phasing system using multiple Segment Piston Sensors (SPS) makes sure that the seven GMT segments remain phased. Simulations have been performed with the Dynamic Optical Simulation (DOS) tool developed at the GMT Project Office, which integrates the optical and mechanical models of GMT. DOS fast ray-tracing capabilities allows us to properly simulate the effect of field-dependent aberrations, and in particular, the so-called Field Dependent Segment Piston (FDSP) mode arising when a segment tilt on M1 is compensated on-axis by a segment tilt on M2. We will show that when using an asterism of SPS, our scheme can properly control both segment piston and the FDSP mode.

Keywords: Giant Magellan Telescope, phasing, wavefront control, numerical simulations

1. INTRODUCTION

The Giant Magellan Telescope (GMT)[1] is a 25.4m diameter aplanatic Gregorian telescope that will be located at the Las Campanas Observatory (LCO), in Chile. The GMT is a segmented telescope, with a primary mirror (M1) composed of seven circular 8.4m segments. GMT will have an Adaptive Secondary Mirror (ASM)[2] composed of seven circular 1.05m segments with deformable thin face sheets, matched 1:1 to the segments of M1.

Phasing the M1-M2 segments to a small fraction of the observing wavelength (0.9-25μm) is only required when operating the GMT in two diffraction-limited Adaptive Optics (AO) modes,[3] namely the Natural Guide star AO (NGAO), and the Laser Tomography AO (LTAO) modes. The Phasing System relies on measurements provided by edge sensors on M1, edge sensors on M2, and multiple natural guidestar Segment Piston Sensors[4] (SPS) deployed across the field of view, plus additional atmospheric piston measurements available only in the NGAO mode.[5] This paper is only concerned with the measurements provided by the set of natural guidestar SPS to address the problem of *field-dependent* segment piston control.

In Sec. 2 we will review the origin of field-dependent aberrations and in particular field-dependent segment piston. In Sec. 3 we will present a preliminary validation of the piston sensing and control strategy using the Dynamic Optical Simulation (DOS) tool.[6] DOS is an end-to-end simulator being developed at the GMT Project Office that integrates the optical and mechanical models of the telescope. As we will show in Sec. 2, the integrated optical model in DOS and its fast (GPU-based) ray-tracing capabilities allow us to properly simulate the effects of field-dependent aberrations.

2. FIELD DEPENDENT SEGMENT PISTON

An aberration $W(\vec{r})$ on M1 compensated on-axis with M2, or vice-versa, leads to a flat wavefront on-axis but to off-axis Field-Dependent Aberrations (FDA) because M1 and M2 are not in optically conjugated planes. The resulting FDA at an off-axis field angle $\vec{\theta}$ can be approximated by:[4]

$$\begin{aligned} W_{FDA}(\vec{r},\vec{\theta}) &= W(\vec{r}) - W(\vec{r}+\Delta\vec{r}) \\ &\approx \Delta\vec{r}\cdot\nabla W(\vec{r}) \ , \end{aligned} \tag{1}$$

Send correspondence to: fquiros@gmto.org

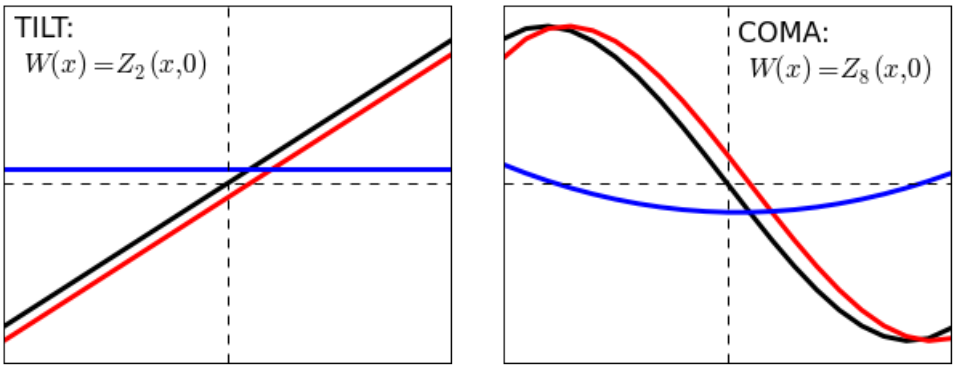

Figure 1. Illustration of the origin of Field-Dependent Aberrations (FDA). The black line represents the profile ($y = 0$) of an aberration $W(x, y)$ present on an M1 segment; x-tilt $Z_2(x, y)$ on the Left, and coma $Z_8(x, y)$ on the Right plot. The red line represents the aberration on the matching M2 segment as seen from an off-axis angle, i.e. $W(x + \Delta x, 0)$. Finally, the blue line represents the resultant FDA, given by $W(x, 0) - W(x + \Delta x, 0)$. Note that the FDA in the case of the x-tilt results in a *Field-Dependent* Segment Piston (FDSP) error, and in the case of coma results in FDSP, focus, and astigmatism (Eq. 3).

where the pupil shift at M2 is $\Delta\vec{r} = a\vec{\theta}$, and the constant a is a function of the telescope optical design parameters. For aberrations defined over one GMT segment, it can be shown[4,7] that $a = 1.11 \times 10^{-2}$ arcmin^{-1}.

Note that the FDA, as a first order approximation, is proportional to the gradient of $W(\vec{r})$. The case that we will be mainly concerned with is a segment tilt whose gradient is a segment piston. In fact, a tilt of an M1 segment compensated by the opposite tilt of the matching M2 segment will result in zero tilt in the focal plane, but a *Field-Dependent Segment Piston* (FDSP) aberration at any other off-axis field angle (Figure 1). This condition is the main source of FDSP, but other low-order aberrations can also produce FDSP. For instance, a coma (Z_7 or Z_8) on an M1 segment compensated by the opposite coma on M2 will generate a FDSP component since:[7]

$$\partial Z_7/\partial y = \sqrt{8}Z_1 + 2\sqrt{6}Z_4 - 2\sqrt{3}Z_6\,, \quad (2)$$

$$\partial Z_8/\partial x = \sqrt{8}Z_1 + 2\sqrt{6}Z_4 + 2\sqrt{3}Z_6\,. \quad (3)$$

Figure 2 shows some examples of FDA simulated with DOS. The initial simulated aberration is just a static $1\mu m$ RMS WF Zernike mode (x-tilt or coma) over an M1 segment. No dynamic disturbances (e.g. atmospheric turbulence, wind buffeting, etc.) will be considered in this paper. The correction of the on-axis AO system (in reality NGAO or LTAO) is for simplicity simulated with a noiseless and low-order AO loop with a 26×26 Shack-Hartmann (SH) sensor driving the shapes of the M2 (ASM) segments. The shape of the ASM is simulated with just 15 Zernike modes per segment in this paper.

As expected, after the on-axis AO loop converges, the static aberration is cancelled on-axis and a FDA arises off-axis. The left of Figure 3 shows that the FDSP simulated results presented in Figure 2 (middle row) are in excellent agreement with the first-order model described by Eq. (1). For the case of coma (bottom row of Figure 2), the Right plot of Figure 3 shows that the Zernike expansion of the simulated FDA contains the expected terms given by Eq. 3, but a higher-order (Taylor) approximation in Eq. (1) would be required to fit the simulated results at large field angles.

3. SEGMENT PISTON CONTROL STRATEGY

A single SPS, while accurately measuring the segment piston at its off-axis position, will not be able to disentangle a *true* segment piston error from a FDSP. Therefore, for the case of tilt-generated FDSP, the accuracy of a single SPS would be a function of the accuracy to which zero relative tilt can be maintained between the telescope segments, leading to stringent long-term stability requirements on edge sensors.[3]

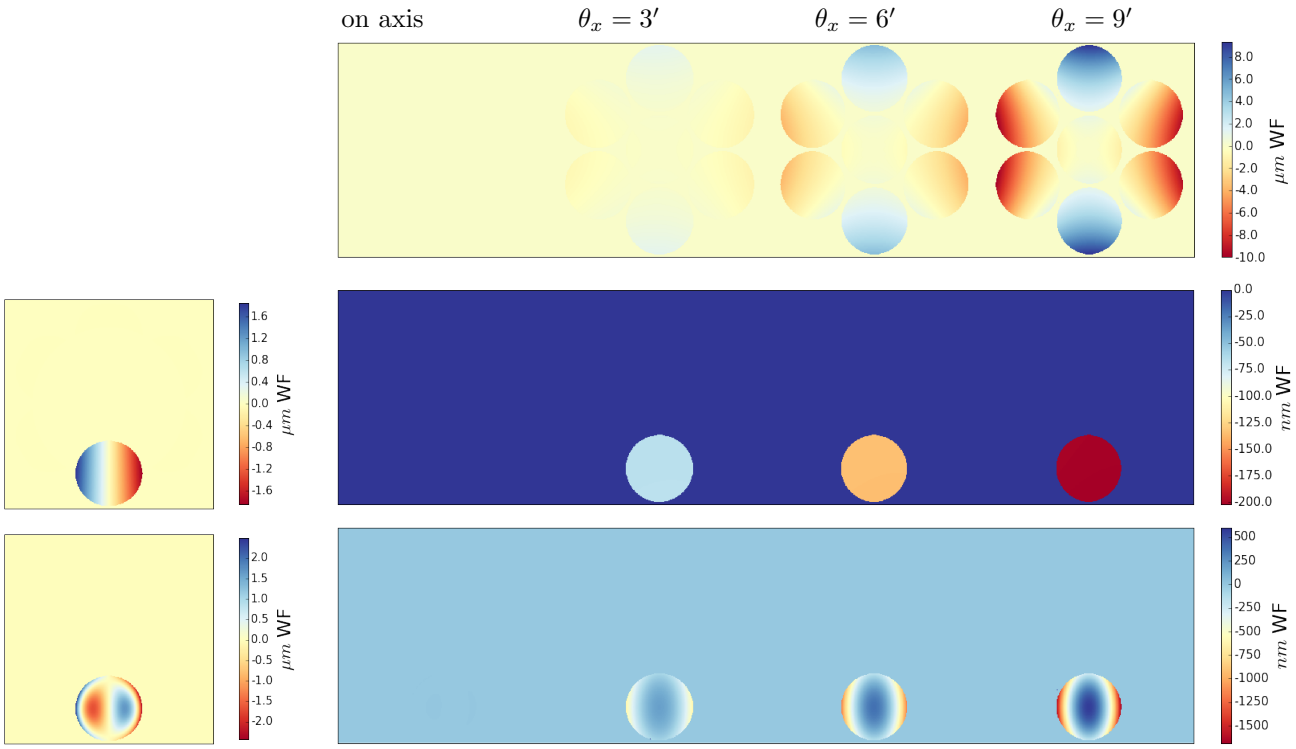

Figure 2. Examples of FDA simulated with DOS at four field angles along the $\theta_y = 0$ axis: on-axis, and off-axis at a distance of $\theta_x = 3$, 6, and 9 arcmin. *Top row*: Telescope nominal field aberrations (i.e. mainly a global quadratic astigmatism); *Middle row*: FDSP arising from a $1\mu m$ RMS WF x-tilt on an M1 segment (shown on the left) compensated by the matching M2 segment (not shown); *Bottom row*: FDA arising from a $1\mu m$ RMS WF coma (Z_8) on an M1 segment (shown on the left) compensated by the matching M2 segment (not shown). Note that telescope nominal aberrations (in the microns range) had to be subtracted from these simulated x-tilt and coma results in order to visualize the FDA.

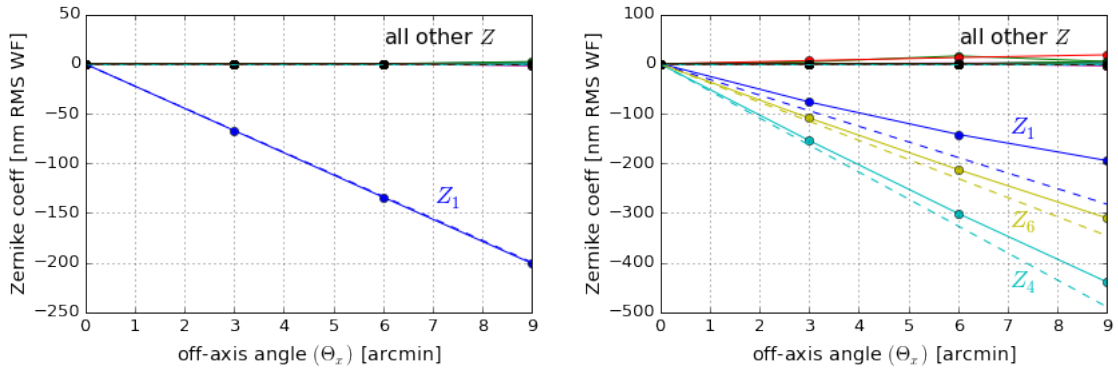

Figure 3. Projection of the FDA onto the first 20 Zernike modes (defined over an outer GMT segment) as a function of the field angle (θ_x), when segment tilt (Left plot) and Z_8 (Right plot) on an M1 segment is compensated by M2. Dashed lines represent the expected FDA values given by Eq. (1). The Circles represent the FDA simulation results shown in Figure 2.

Instead, a set of at least three SPS deployed across the field of view would be able to disentangle a *true* segment piston from a FDSP error, because the former does not vary in the field. This approach is part of the current baseline design of the GMT phasing system, with four SPS integrated in the Acquisition, Guiding, and Wavefront sensing System (AGWS) probes, which can be positioned in the field between 6' and 10' radius off-axis.[4]

We will consider in the following simulations the wavefront sensing configuration shown on the Left of Figure 4. As in the previous section, the correction of the on-axis AO system is simulated with a noiseless and low-order AO loop with a 26×26 SH sensor driving the shapes of the M2 (ASM) segments (with 15 Zernike modes per segment).

For segment piston and FDSP control, we will use a set of three SPS located in a circle of 6 arcmin radius, as illustrated on the Left of Figure 4. The nature of the SPS and its implementation in DOS will be briefly described in Sec. 3.1. The calibration procedures of segment piston and FDSP will be presented in Sec. 3.2. Finally, we will present in Sec. 3.3 a preliminary closed-loop validation of the piston sensing and control strategy using the DOS.

3.1 Dispersed Fringe Sensors

The baseline design of the SPS for GMT is based on a Dispersed Fringe Sensor (DFS) operating with broadband light in J band.[4,8] We have implemented a full Fourier-optics model of the DFS in DOS. Each DFS has twelve 1.5m×1.5m lenslets located across the gaps between segments, as shown on the Right of Figure 4. The lenslets are conjugated to a plane half-way between M1 and M2 to cope with vignetting effects.[8] The light collected by each lenslet is dispersed by a grism in the direction parallel to the segment gap and the resulting fringes are imaged on a detector. The dispersion in the bandpass is simulated by adding a corresponding wavelength-dependent tilt.

A differential piston between two segments causes an apparent tilt in the fringes. The actual differential piston estimate is retrieved from the modulus of the Fourier Transform of the fringes. The tilt in the fringes is translated in the Fourier domain into a displacement of the side lobes in the direction perpendicular to the *reference* axis (Fig. 5). This displacement varies linearly with the differential piston, and the sensitivity depends on the grism dispersive power (5 arcsec/micron in these simulations). In practice, it is just required to estimate the displacement of one side lobe. Hence, the signal vector delivered by the DFS is a 12-element vector containing the side-lobe displacement measurements of all subapertures.

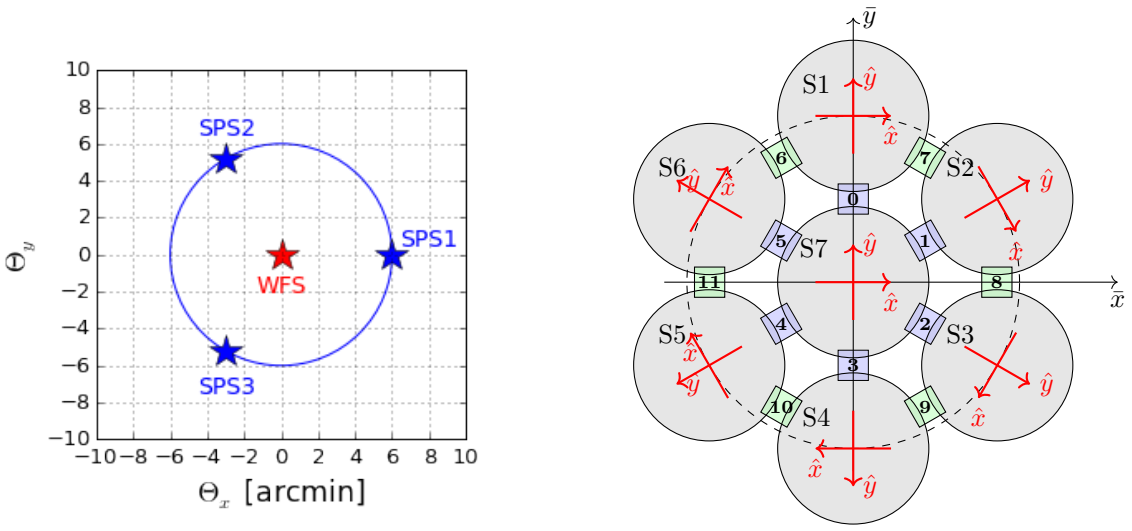

Figure 4. (Left) Wavefront sensing configuration comprised of an on-axis SH WFS and a set of three SPS located in a circle of 6' radius. (Right) Illustration showing the location and numbering of the 12 SPS subapertures.

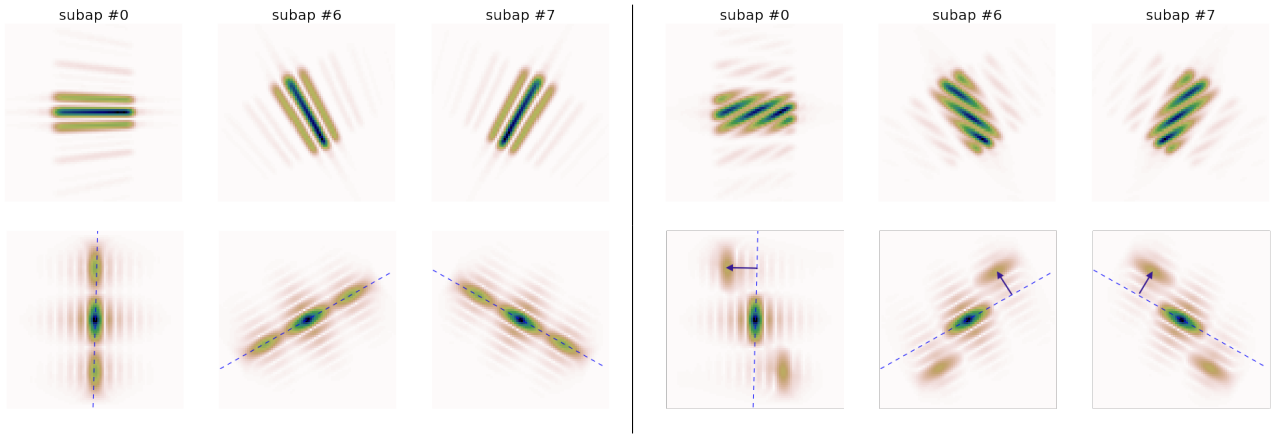

Figure 5. Examples of fringes (Top row) and the moduli of their Fourier Transforms (Bottom row) in noiseless conditions for the three DFS subapertures (#0, #6, #7) across the gaps of segment S1 (see the Right of Fig. 4). The set of images on the Left is for the simulated phased condition. Note that the three lobes in the Fourier images are aligned along a so-called *reference* axis (dashed blue line). The set on the Right corresponds to the case of a 16 μm WF segment piston on S1. Note that the fringes are tilted, and that the side lobes in the Fourier images are displaced in the direction perpendicular to the reference axis.

3.2 Interaction matrices calibration

We will focus in this section on the calibration of interaction matrices involving the SPS. We will show that the proper estimation of *true* segment piston and FDSP from the set of SPS measurements can be done with the use of a single reconstruction matrix, computed as the generalized inverse of the concatenation of two interaction matrices:

$$\mathbf{R} = [\mathbf{M}_{_{SP}}\, \mathbf{M}_{_{FDSP}}]^{\dagger} \,, \tag{4}$$

where $\mathbf{M}_{_{SP}}$ stands for the segment piston interaction matrix (IM), and $\mathbf{M}_{_{FDSP}}$ stands for the FDSP IM.

The segment piston IM (Left of Fig. 6) can be calibrated with a standard procedure, i.e. applying piston to a segment at a time and acquiring the SPS measurements. Note that the central segment (S7) won't be included in the IM calibrations since it will serve as the reference for measuring the outer segment differential pistons.*

The calibration of the FDSP IM requires an ad-hoc procedure with the following steps: 1) Apply a know tilt on an M1 segment; 2) Compensate on-axis for the M1 segment tilt with the matching M2 segment. In practice, this could be done by closing the on-axis AO loop driving the M2 to compensate for the introduced M1 segment tilt; 3) Acquire the SPS measurements after the previous step converged.

The FDSP IM is shown on the Right of Figure 6. Note that, for each degree of freedom (S1 R_x, $\cdots$, S6 R_y), the measurements of the three SPS are different, as opposed to the case of the segment piston IM, for which the three SPS measurements do not vary in the field. Hence, the reconstruction matrix $\mathbf{R}$ represents a well-conditioned inverse problem that enables the estimation of both segment piston and FDSP without crosstalk. In the following section we will test the performance of this reconstruction approach in a preliminary closed-loop simulation.

3.3 Segment piston control: preliminary validation

We will present in this section a preliminary simulation result thats validates the piston sensing and control strategy in the absence of dynamic disturbances. Recall that the wavefront sensing configuration was shown on the Left of Figure 4. Two control loops running in parallel have been simulated: an on-axis (low-order) AO loop driving the shapes of the M2 segments (up to 15 Zernike modes per segment), and a phasing loop running 5 times slower controlling segment piston and FDSP.

*This is an arbitrary choice. If the central segment is included in the IM calibration, a global piston mode must be filtered out in the SVD inversion.

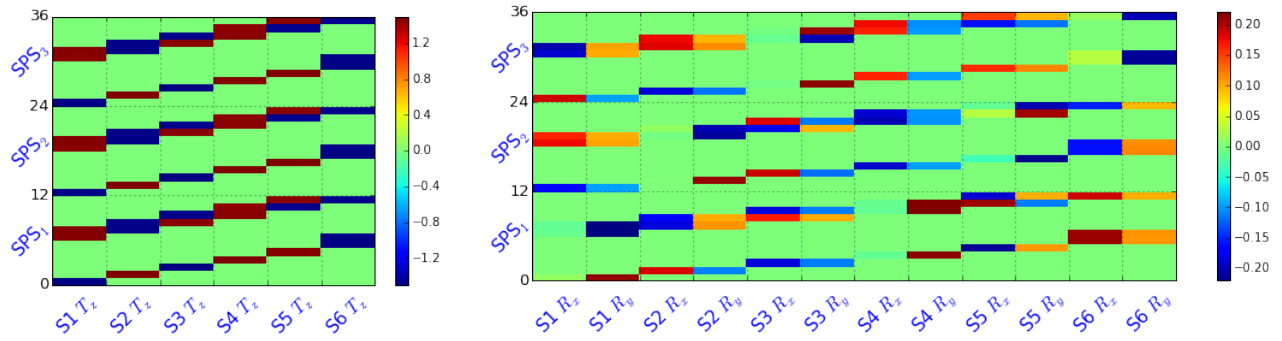

Figure 6. (*Left*) M1 segment piston interaction matrix ($\mathbf{M}_{SP}$): T_z represents a translation in the segment $\hat{z}$ axis (Fig. 4). The IM units are in (side lobe) displaced pixels per micron SURF of M1 segment piston. (*Right*) FDSP interaction matrix ($\mathbf{M}_{FDSP}$): R_x and R_y represent an M1 segment rotation about the local $\hat{x}$ and $\hat{y}$ axes, respectively (Fig. 4). The IM units are in (side lobe) displaced pixels per micron RMS SURF of M1 segment tilt.

Since this preliminary simulation is noiseless the actual sampling rates are not relevant, but in practice, the NGAO loop will be running at a maximum of 1kHz whereas the SPS in the AGWS unit will be delivering measurements every 30 seconds.[3]

Figure 7 shows the wavefront control loop convergence in terms of global on-axis WFE versus the control iteration number. The initial static disturbance on M1 consists of $4\mu m$ WF of segment piston on S1, and $4\mu m$ RMS WF of y-tilt on S4. When the AO loop is closed the M2 is driven to compensate for the tilt on the M1 segment. As a result, the on-axis residual WF (shown in Fig. 7 at iteration #4) over S4 is nulled. The only remaining error at iteration #4 is the M1 segment piston on S1, which the AO SH WFS cannot see.

At iteration #5 the three SPS provide a set of measurements that contain information on both the segment piston on M1 S1, and on the FDSP formed over S4 due to the tilt on M2 S4 compensating the tilt on M1 S4. The application of the correction computed with the reconstructor $\mathbf{R}$ leads to the nulling of the S1 piston, and to the nulling of the M1 S4 tilt that caused the FDSP. Note that the residual WF at this point (shown in Fig. 7 at iteration #5) over S4 is actually the tilt on M2 that shows up once the opposite tilt on M1 is removed. Of course, all of these steps do not happen in reality in a single instant, as simulated here, but spans some time in particular when considering also the dynamics of M1 and loop delays.

Finally, the remaining M2 S4 tilt is cancelled by the AO loop (iterations #6 and #7) and, after another iteration of the phasing correction (at iteration #10), the WF error is completely nulled. Note that the final WFE is just 0.79 nm WF RMS of a global spherical, as expected from the optical design of GMT.

3.4 Aliasing errors on segment piston estimation

We mentioned in Sec. 2 that a coma (Z_7 and Z_8) on an M1 segment compensated by the opposite coma on M2 also produces a FDSP component (Eq. 2 and 3). We could in principle extend our interaction matrix calibration approach described in Sec. 3.2, so that the IM $\mathbf{M}_{FDSP}$ would contain additional columns capturing the SPS measurements produced by the coma-generated FDSP. It would be possible then to control the coma over M1 segments, in the same way as M1 segment tilt, to null the associated FDSP error. We do not foresee to implement this approach, and so any coma on M1 compensated by M2 will be aliased onto segment piston and tilt-generated FDSP modes.

We present in this section a preliminary quantification of the error introduced by this condition using DOS. All wavefront sensing and control parameters in the simulation presented in Section 3.3 are still applicable. Figure 8(a) shows the initial static disturbance on M1 consisting of $1\mu m$ RMS WF of segment coma Z_8 on S1. Figure 8(b) shows the wavefront control loop convergence in terms of global on-axis WFE versus the control iteration number. When the on-axis AO loop is closed, the M2 is driven to compensate for the coma on the M1 S1 segment, taking four iterations to achieve this.

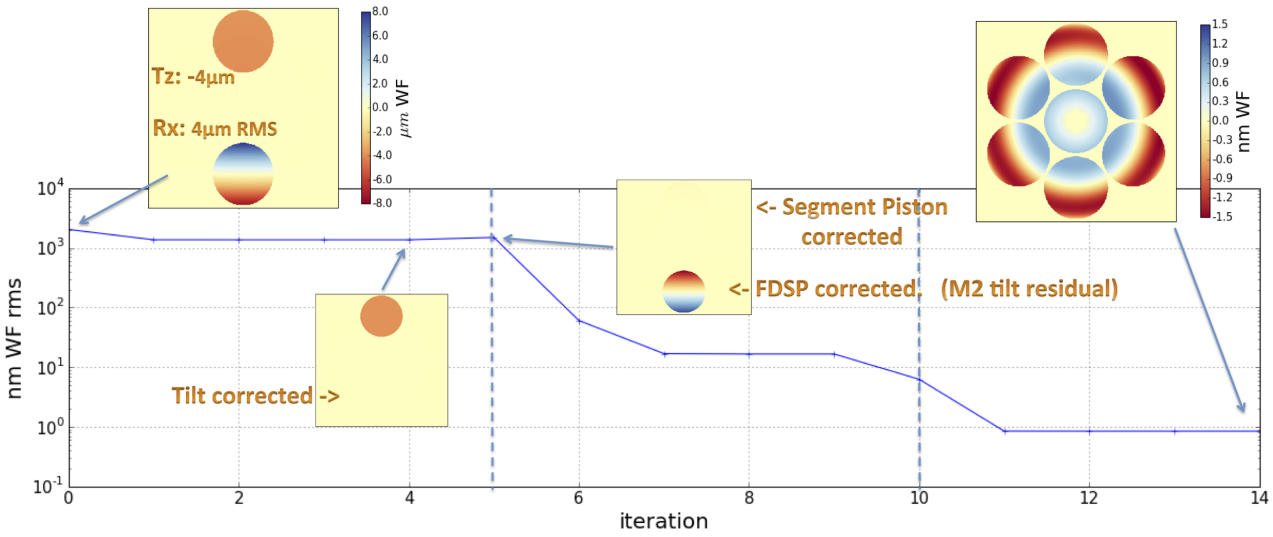

Figure 7. Wavefront error (WFE) in nm WF RMS versus the loop iteration. In this simulation, the AO loop provides a correction every iteration whereas the phasing loop delivers one correction every 5 iterations (indicated with vertical dashed lines). The residual WF is explicitly shown at iterations #0, 4, 5, and 14.

At iteration #5 the first command of the phasing loop is applied, computed from the measurements of the three SPS multiplied by the reconstructor $\mathbf{R}$ in Eq. (4). Ideally, this command should be null, since there is no pure segment piston nor tilt-generated FDSP to compensate for. In practice, aliasing of the coma-generated FDA results in the M1 segment piston and tilt commands shown at iteration #5 in Figures 8(c, d, e). Note that this phasing command introduces erroneous segment piston and segment tilt on all the six (S1-S6) M1 segments. The introduced M1 segment tilt will be seen by the AO WFS and corrected on-axis with M2 in the following iterations (i.e. #6 - #8) whereas the segment piston, to which the AO WFS is blind, will accumulate and contribute to the WFE shown in Figure 8(b).

The on-axis WFE converges, after three phasing control iterations (applied at loop iterations #5, 10, and 15), to a value of 4.4 nm WF RMS (Figure 8(b)). The M1 segment piston, and M1 segment tilts (compensated on-axis by M2), all due to aliasing effects, converged to the values reported in Figures 8(c, d, e).

The remaining WFE in the field due to errors in the FDSP control must also be evaluated. For this particular simulation, the WFE in the field has contributions from: 1) coma-generated FDA on S1; and 2) FDSP on all segments (S1 to S6) generated by M1 tilts compensated by M2. Figure 9 shows the WFE in a field of 1.5' × 1.5'. At the edge of the field, the remaining WFE (after subtracting the WFE due to the nominal telescope aberrations) is ≈48 nm RMS. The amount of acceptable WFE in the field due to residual FDA, and in particular residual FDSP, will depend on instrument requirements. For example, for the case of GMTIFS,[9] a first-generation instrument for GMT, the requirement is to maintain the 29 arcsec diameter science field phased to <50 nm RMS at its edges. Current simulation efforts at GMTO are being conducted to verify this kind of performance requirements.

The analysis in this section focused on the aliasing effects of coma, one particular mode that produces a FDSP component, similar to segment tilt. Even if other modes like astigmatism do not generate a FDSP, they may also produce aliasing errors because they will be sampled by the SPS subapertures in just a small portion of the pupil over which the average differential piston may not be zero. The quantification of aliasing error contributions from other low-order modes of relevance (e.g. active optics residuals compensated by the ASM) will be done as a next step of this study.

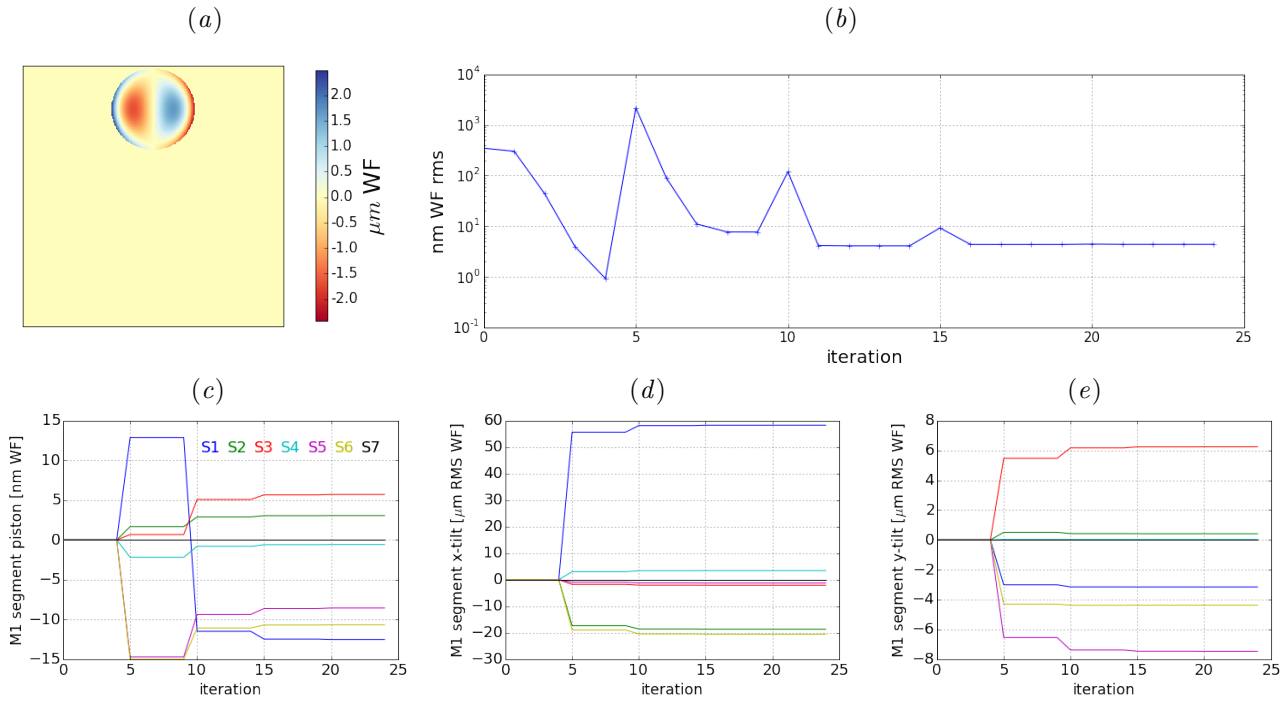

Figure 8. (a) Initial static aberration on M1 with a $1\mu m$ RMS WF coma (Z_8) on S1. (b) On-axis WFE in nm WF RMS versus the loop iteration. (c) M1 segment piston commands versus the loop iteration. (d) M1 x-tilt commands versus the loop iteration. (e) M1 y-tilt commands versus the loop iteration.

4. CONCLUSIONS AND FUTURE WORK

In this paper we have presented a preliminary validation of the segment piston and FDSP wavefront sensing and control strategy for GMT. We have shown that with three SPS distributed in the field, and using an ad-hoc calibration procedure, these modes can be measured, disentangled, and controlled. We have also performed a preliminary analysis of the aliasing error of coma-generated field dependent aberrations. All of these simulations have been performed in the absence of noise and dynamic disturbances. As a future work, we will include these perturbations in our simulations and evaluate the phasing errors in the field of view of interest under different observing conditions.

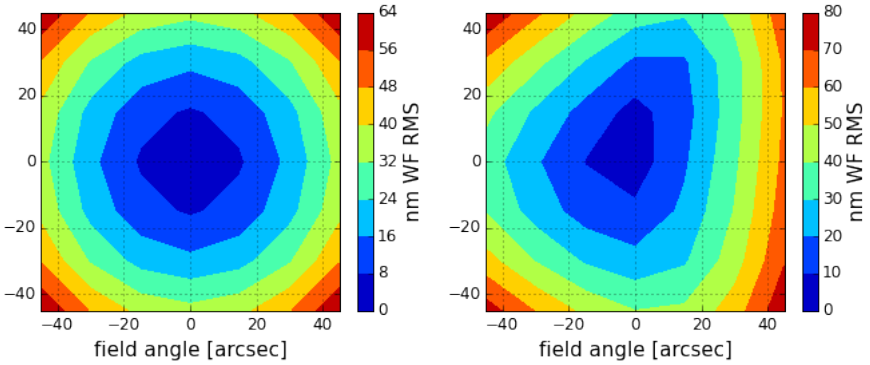

Figure 9. WFE in the 1.5' × 1.5' field: (*Left*) Nominal WFE for a perfectly aligned telescope; (*Right*) WFE map resulting from the simulation presented in Figure 8.

REFERENCES

[1] "Giant Magellan Telescope website." http://www.gmto.org.

[2] Biasi, R., Veronese, D., Andrighettoni, M., Angerer, G., Gallieni, D., Mantegazza, M., Tintori, M., Lazzarini, P., Manetti, M., Johns, M. W., Hinz, P. M., and Kern, J., "GMT adaptive secondary design," *Proc. SPIE* **7736**, 77363O (2010).

[3] Bouchez, A. H., Acton, D. S., Biasi, R., Conan, R., Espeland, B., Esposito, S., Filgueira, J. M., Gallieni, D., McLeod, B. A., Pinna, E., Santoro, F., Trancho, G., and van Dam, M. A., "The Giant Magellan Telescope adaptive optics program," *Proc. SPIE* **9148**, 91480W (2014).

[4] McLeod, B. A., Kopon, D., van Dam, M. A., and Bouchez, A. H., "An off-axis segment piston sensor for the Giant Magellan Telescope," *these AO4ELT4 conference proceedings* (2015).

[5] Pinna, E., Agapito, G., Quirós-Pacheco, F., Antichi, J., Carbonaro, L., Briguglio, R., Bonaglia, M., Riccardi, A., Puglisi, A., Biliotti, V., Arcidiacono, C., Xompero, M., Di Rico, G., Valentini, A., Bouchez, A., Santoro, F., Trancho, G., and Esposito, S., "Design and numerical simulations of the GMT Natural Guide star WFS," *Proc. SPIE* **9148**, 91482M (2014).

[6] Conan, R., Bouchez, A. H., Quirós-Pacheco, F., and McLeod, B. A., "The Giant Magellan Telescope Dynamic Optical Simulation tool," *these AO4ELT4 conference proceedings* (2015).

[7] McLeod, B. A., "Analytic treatment of compensated M1/M2 aberrations," Tech. Rep. version 1.2, Smithsonian Astrophysical Observatory (October 2015).

[8] van Dam, M. A., McLeod, B. A., and Bouchez, A., "Measuring segment piston with a Dispersed Fringe Sensor on the Giant Magellan Telescope," *these AO4ELT4 conference proceedings* (2015).

[9] McGregor, P. J., Bloxham, G. J., Boz, R., Davies, J., Doolan, M., Ellis, M., Hart, J., Jones, D. J., Luvaul, L., Nielsen, J., Parcell, S., Sharp, R., Stevanovic, D., and Young, P. J., "GMT integral-field spectrograph (GMTIFS) conceptual design," *Proc. SPIE* **8446**, 84461I (2012).